

Near 100% surface transport in topological insulator  $\text{Bi}_{1.5}\text{Sb}_{0.5}\text{Te}_{1.8}\text{Se}_{1.2}$   
single crystalline nanoflake device

Bin Xia<sup>1</sup>, Ming-Yi Liao<sup>1</sup>, Peng Ren<sup>1</sup>, Azat Sulaev<sup>1</sup>, Shi Chen<sup>1</sup>, Cesare Soci<sup>1</sup>, Alfred Huan<sup>1</sup>, Andrew TS Wee<sup>2</sup>, Andriwo Rusydi<sup>2</sup>, Shun-Qing Shen<sup>3</sup>, Lan Wang<sup>1\*</sup>

1. *Nanyang Technological University, School of Physical and Mathematical Science, Singapore, 637371*
2. *National University of Singapore, Department of Physics, Singapore 117542, Singapore*
3. *University of Hong Kong, Department of Physics, Pokfulam, Hong Kong, People's Republic of China*

We synthesized high quality topological insulator  $\text{Bi}_{1.5}\text{Sb}_{0.5}\text{Te}_{1.8}\text{Se}_{1.2}$  single crystals with huge bulk resistivity via modified Bridgeman method. Nano-devices were fabricated by 200 nm thick  $\text{Bi}_{1.5}\text{Sb}_{0.5}\text{Te}_{1.8}\text{Se}_{1.2}$  exfoliated flakes. Angle-dependent magneto-resistance curves of the nanoflake devices merge to a universal curve when the x-axis is the perpendicular component of the applied magnetic field. A fit to the 2D weak antilocalization theory for the nanoflake device gives  $\sim T^{-0.51}$  dependence of the phase breaking length ( $< 200$  nm) on temperature within 2 Tesla field. A time dependent universal conductance fluctuation was observed in the nanoflake devices. All the experimental results indicate that near 100% surface transport is realized in the 3D 200 nm thick nanoflake devices.

\*Email: wanglan@ntu.edu.sg

PACS numbers: 73.25.+i, 73.20.Fz, 72.20.My, 73.23.-b

Topological insulators (TIs) are a new phase of insulators which are gapped bulk insulators with gapless Dirac surface states [1,2]. The surface states (SS) of these topological insulators are spin polarized and protected by time reversal symmetry. Angle-resolved photoemission spectroscopy (ARPES) [3-5] and scanning tunneling microscopy[6-8] have been used to detect the topologically nontrivial SS in 3D topological insulator  $\text{Bi}_{1-x}\text{Sb}_x$ ,  $\text{Bi}_2\text{Se}_3$ ,  $\text{Bi}_2\text{Te}_3$ , *etc.* The spin polarization of the SS has been confirmed by spin-resolved ARPES [9-13]. In addition to the surface sensitive probes, transport experiments are important for studying the properties of TIs and exploiting the applications based on the novel SS. However, bulk  $\text{Bi}_2\text{Se}_3$  samples always show the heavily doped n-type behavior due to the Se vacancies while bulk  $\text{Bi}_2\text{Te}_3$  is prepared as p-type due to the anti-site defects, which contribute large bulk conductance. Therefore, it is challenging to observe the SS from 3D bulk signals by electron transport in the two material systems [14-19]. Reducing the thickness of samples and chemical doping are the effective methods for decreasing the bulk signals. The electron transport characterizations on ultra thin topological insulator films and nanostructures have been widely carried out. Surface transport induced Aharonov-Bohm oscillation has been observed in  $\text{Bi}_2\text{Se}_3$  nanowire [20].  $\pi$  Berry phase and strong spin-orbit interaction induced weak antilocalization (WAL) on the exotic topological surface state has been thoroughly studied in  $\text{Bi}_2\text{Se}_3$  and  $\text{Bi}_2\text{Te}_3$  thin films and nanostructures [16,21-25]. However, as all the previous WAL studies are based on ultra thin films, the 3D topological insulator system is in fact a 2D transport system for WAL transport measurements, because the phase breaking length is larger

than the thickness of the thin film. Both the bulk and helical surface contribute to the 2D WAL transport. No one has ever measured a 2D WAL in a 3D transport system (the phase breaking length  $>$  the thickness of sample). The electrical transport measurements have also been carried out on various doped  $\text{Bi}_2\text{Se}_3$  bulk single crystals. For example, the universal conductance fluctuations (UCF) coming from the SS were observed in Ca-doped  $\text{Bi}_2\text{Se}_3$  bulk single crystals [17]. Recently, new topological insulator  $\text{Bi}_2\text{Te}_2\text{Se}$  [26-28] and  $(\text{Bi}_{1-x}\text{Sb}_x)_2(\text{Te}_{1-y}\text{Se}_y)_3$  [29-31] single crystals with huge bulk resistivity (1 - 10  $\Omega$  cm) and dominated surface transport have been synthesized. These materials offer a well characterized play ground for studying the topological surface state.

In this letter, we report the study of WAL and UCF on  $\text{Bi}_{1.5}\text{Sb}_{0.5}\text{Te}_{1.8}\text{Se}_{1.2}$  (BSTS) single crystalline nanoflake devices. We synthesized high quality BSTS single crystal with huge bulk resistivity via modified Bridgeman method. Nano-devices were fabricated by 200 nm thick BSTS exfoliated flake. In order to probe the 2D surface transport, we measured and compared the angle-dependent and temperature-dependent magnetoresistance curves of bulk single crystal and nanoflakes. It was found that  $R$  vs  $B\sin\theta$  of the nanoflake devices merge to a universal curve, where  $\theta$  is the angle between the applied magnetic field and current flowing plane. WAL effect was observed in both BSTS bulk single crystal and nanoflake devices. The power law dependence of the phase breaking length  $L_\phi$  ( $< 200$  nm) on temperature is  $\sim T^{-0.51}$  within 2 Tesla field. A time-dependent UCF was observed in the

nanoflake device. Although UCF has been reported in  $\text{Bi}_2\text{Se}_3$  single crystal [17] and thin films [32], time-dependent UCF is observed for the first time in topological insulator. All the experimental results indicate that near 100% surface transport is realized in the 3D 200 nm thick nanoflake device (the phase breaking length  $L_\phi <$  the sample thickness). The realization of 2D WAL in 3D transport system is very different from previous WAL studies in 2D thin film and nanostructure TIs, where the sample thickness was smaller than the phase-breaking length.

High quality BSTS single crystals were grown using modified Bridgeman methods. The obtained crystals are easily cleaved and reveal a flat and big shiny surface. Angle-resolved photoemission spectroscopy (ARPES) was performed with a VG Scienta R4000 electron analyzer at the SINS beamline at Singapore Synchrotron Light Source (SSLS). The angular and temperature dependent magnetoresistance of a 100  $\mu\text{m}$  thick bulk single crystal and 200 nm thick nanoflake devices were measured. The nanoflakes were mechanically exfoliated from the BSTS single crystal used for the bulk transport measurement.

The resistivity was measured with the applied current in the (001) plane. The temperature dependence of the resistivity of the bulk and nanoflake samples measured in zero field are shown in Fig. 1a and Fig. 1b. The 100  $\mu\text{m}$  thick bulk crystal shows semiconductor behavior in the whole temperature regime and starts a saturation behavior when  $T < 40$  K. The resistivity at 10 K is more than 200 times larger than

that at room temperature. Although the nanoflake device also shows the semiconductor behavior in high temperature range, the transport characteristics transfer to metallic type when  $T < 150$  K. It should be noted from Fig. 1a and 1b that the resistivity of nanoflake is  $\sim 250$  times smaller than that of the bulk single crystal although the nanoflake was exfoliated from the bulk crystal used in the transport measurement (Fig. 1a). This indicates that the SS contribution plays a more and more important role as the thickness reduced. Suppose the thickness of SS is 5 nm, we can easily conclude that the resistivity of the SS is smaller than  $1 \text{ m}\Omega \text{ cm}$  and the conductance contribution of the SS is higher than 99% at 10 K. Near 100% SS transport can be realized when the nanoflake is several hundred nanometer thick. The inset of Fig. 1a shows the ARPES spectrum of the BSTS single crystal at room temperature. The Dirac cone structure similar to the results in a very recent literature can be observed [29]. The inset of Fig. 1b shows the morphology of the nanoflake device under Scanning Electron Microscopy.

To further confirm the 2D electron transport in the nanoflake device, we performed the angular dependent magnetoresistance measurements. The magnetoresistance was measured by tilting the bulk crystal and nanoflake device with respect to the applied magnetic field from  $0^\circ$  to  $90^\circ$ . The  $\theta = 0^\circ$  means the magnetic field parallel to the (001) surface while the  $\theta = 90^\circ$  means the magnetic field perpendicular to the (001) surface. Fig. 2a and 2b show the  $R(H)$  curves with various  $\theta$  for bulk single crystal and nanoflake device at 2K respectively. Both bulk and nanodevice show the weak

antilocalization (WAL) behavior in the low magnetic field region. Such WAL at low temperature has been proved to be induced by both strong spin-orbital coupling and topological  $\pi$  Berry phase of 2D surface states [33]. It is very obvious that  $\Delta R(H)/R(0)$  ratio decreases with decreasing  $\theta$  for both bulk single crystal and nanoflake device. The decrease of  $\Delta R(H)/R(0)$  with decreasing  $\theta$  is more pronounced for the nanoflake device. The perpendicular component of the magnetic field dependence of the variation of magnetoconductance for the bulk single crystal and nanoflake device in  $e^2/h$  unit are shown in Fig. 2c and 2d respectively. All the  $G$  vs  $B\sin\theta$  (the perpendicular component of the applied field) curves of the nanoflake device are merged into one universal curve, which strongly supports the near 100% SS electron transport in the nanoflake BSTS. For the bulk single crystal, the magnetoconductance is due to both the SS and the 3D bulk, therefore the  $G$  vs  $B\sin\theta$  curve cannot be plotted as one universal curve. It is not a surprise that the WAL is observed for all the angles in bulk because of the coexistence of both the 3D bulk spin-orbit coupling effects and helical surface state contribution.

WALs at different temperature (2 K, 4 K, 7 K, 10 K, 15 K, 35 K, and 40 K) have been measured with the magnetic field perpendicular to (001) plane ( $\theta = 90^\circ$ ), as shown in figure 3a and 3b for bulk single crystal and nanoflake device respectively. The magnetoconductance at different temperatures,  $\Delta G = G(B) - G(0)$ , are plotted in these two figures. The Hikami-Larkin-Nagaoka (HLN) formula

$$\Delta\sigma_{2D} = \left[ -\frac{\alpha e^2}{2\pi^2\hbar} \right] \left[ \ln\left(\frac{\hbar}{4eL_\phi^2 B}\right) - \Psi\left(\frac{1}{2} + \frac{\hbar}{4eL_\phi^2 B}\right) \right]$$

is used to fit the weak antilocalized magnetoconductance observed in both bulk and nanoflake device, where  $\Delta\sigma_{2D}$  being the 2D sheet conductance,  $\Psi$  being the digamma function,  $L_\phi$  being the phase breaking length, and  $\alpha$  being a prefactor which contains information about the nature of the electrons in topological insulators [34]. The fitted curves are shown in Fig. 3(a) and 3(b) in solid lines. Due to the 3D bulk contribution, the fitting curves do not agree well with experiment data for bulk single crystal samples in the field up to 2T. For the nanoflake device, the 2D WAL fitting curves agree very well up to 2 Tesla with the experimental data at all temperatures from 2 K to 45 K. The fitting results of  $L_\phi$  and  $\alpha$  for bulk single crystal and nanoflake device are shown in figure 3c, 3d, 3e, and 3f respectively.

Due to the intermixing of bulk and surface interactions in bulk single crystal samples, the phase breaking length  $L_\phi$  and  $\alpha$  fitted by the 2D WAL theory may not be able to reveal detailed physics, while the  $L_\phi$  and  $\alpha$  values fitted from nanoflake device are reliable and illuminating. The phase breaking length  $L_\phi \propto \sqrt{D\tau_\phi}$ , where  $D$  is the diffusion coefficient and  $\tau_\phi$  is the phase breaking time or the mean time between inelastic events which is dependent on temperature. Generally,  $\tau_\phi \propto T^{-p}$  where  $p = 1$  [35]. Thus, we use power law to fit the collected temperature dependent  $L_\phi$  and the fitting result is shown as the red solid line in Fig. 3(d), which gives  $L_\phi \propto T^{-0.51}$  for the nanoflake device. In 2D electron-electron scattering system, the power law dependence should be  $T^{-1/2}$ . Hence, this is another evidence supports that the origin of

WAL features of device is from 2D surface states. It should be noted that the fitted  $L_\phi$  at all temperatures are smaller than the thickness of the sample (200 nm), which strongly indicates that 2D electron transport characteristics are due to the helical SS. From this point of view, our experiment is very different from previous WAL measurements on ultra thin  $\text{Bi}_2\text{Se}_3$  and  $\text{Bi}_2\text{Te}_3$  films. The 2D transport behavior in ultra thin  $\text{Bi}_2\text{Se}_3$  and  $\text{Bi}_2\text{Te}_3$  films cannot be attribute to the surface state, because the  $L_\phi$  is larger than the thickness of the film and therefore the film itself, including the bulk and surface, form a 2D transport system. Since the thickness of our nanoflake BSTS device is larger than  $L_\phi$ , it is a 3D transport system for WAL. The 2D WAL transport behavior can only come from the helical surface state.

The coefficient  $\alpha$  takes a value of -1/2 for a traditional 2D electron system with strong spin-orbit coupling. For the electron transport on one helical surface with a single Dirac cone,  $\alpha$  is also equal to -1/2. Since carriers on both up and bottom surface can contribute the conduction in topological insulator samples, double transport channel should add up to give  $\alpha = -1$ . In previous WAL studies in topological insulator, due to the ultrathin film and large bulk contribution, the interactions between two surfaces and the intermixing of multiple conductance channels from bulk and surface bands at Fermi surface can introduce a correction to WAL which let  $\alpha$  differ from -1. The experimental fitted  $\alpha$  covers a range between -0.4 and -1.1. Our fitted  $\alpha$  at different temperatures is plotted in Fig 3(e) and (f). The fitted  $\alpha$  values deviate from -1 for both bulk and nanoflake device at all temperatures. As the negative magnetoconductance



behavior of bulk single crystalline BSTS cannot be fitted well using the 2D HLN formula, it is not a surprise that the fitted value is far away from the theoretical value of -1. For the nanoflake device, the perfect fitting using HLN formula generates  $\alpha$  values between -0.7 to -0.85 for different temperatures. The deviation from -1 may come from other effects, such as the warping of the Dirac cone.

We also observed a novel conductance fluctuation phenomenon in the nanoflake device under both low and high magnetic fields. The low magnetic field conductance fluctuation is very clear as shown in Fig. 2b and 2d. Fig. 4a shows the conductance fluctuations at different temperatures below 10 K between 4 Tesla and 9 Tesla perpendicular field. Different from normal universal conductance fluctuations (UCF) discovered in topological insulator  $\text{Bi}_2\text{Se}_3$  [17,32], the conductance fluctuation in our nanoflake device evolves with time. Such time-dependent UCF can only be observed below 10 K and the magnitude of those fluctuations increases with decreasing temperature. The top 3 curves shown in Fig. 4 (a) were measured continuously with different field sweeping direction without stop. As shown in the circled region in the figure, the curves show very similar fluctuation behaviors in the same magnetic field region because the time interval between the measurements is short. With the time evolution, the fluctuation patterns become more and more different in the same magnetic field region. Time dependent UCF is due to the enhanced sensitivity of the conductance to the motion of individual scatters and such phenomena has been reported [36]. The variation of conductance pattern is due to the motion of scattering

sites which changes the interference pattern of all the intersecting electronic paths in the coherent volume of the scattering sites. Since the motion of scattering site is related to the time, the observed fluctuations are also time dependent which allows the non-retraceable results. As the electron transport in the nanoflake is almost fully surface transport as discussed before, the motion of the scattering site might be due to the time dependent surface contamination in the measurement chamber. Each MR curve from 4 Tesla to 9 Tesla takes about 1 hour. According to the results, we can conclude that the scattering site pattern on the topological surface changes after 30 minutes.

The amplitude of fluctuation detected is around  $0.2e^2/h$ . The phase breaking length of electron  $L_\phi$  observed at 2 K is  $\sim 0.18 \mu\text{m}$  (Fig. 3d) and the thermal length,  $L_T = \sqrt{\frac{\hbar D}{k_B T}}$

is around  $1 \mu\text{m}$  at 2 K. As  $L_\phi < L_T < L$ , the fluctuation of  $G$  can be calculated[37] as

$$\delta G = \frac{e^2}{h} \left[ \frac{L_\phi}{L} \right]^{4-d}, \text{ where } L \text{ is the sample size. The calculated } \delta G \text{ is } 0.3e^2/h \text{ which is}$$

quite agreeable with our experiment data  $0.2e^2/h$  at 2 K. Furthermore, the root-mean-square (rms) of  $\delta G$  vs temperature curve is also plotted as shown in Fig 4b. The rms of  $\delta G$  is usually following the power law  $\text{rms} \delta G \propto T^{-0.5}$  for two dimensional system. Our fitting shows  $\text{rms} \delta G \propto T^{-0.43}$ , which also indicates that the time-dependent UCF observed in the BSTS device sample is mainly from 2D SS.

In conclusion, we successfully synthesized high quality BSTS topological insulator

single crystal with huge bulk resistivity and fabricated nanoflake BSTS device with negligible bulk transport contributions. We observed WAL effect in both BSTS bulk single crystal and nanoflake devices. Further study shows that such phenomena origins from 2D surface states for nanoflake devices and intermixing of surface states and 3D bulk spin-orbital couplings for bulk single crystals. A time dependent universal conductance fluctuation was observed in the nanoflake device. Our results indicate that near 100% SS electron transport has been realized in nanoflake BSTS devices, which form a perfect play ground for future study of the electron and spin transport on topological helical surface states.

Support for this work came from Singapore National Research Foundation (RCA-08/018) and MOE Tier 2 ( MOE2010-T2-2-059).

- [1] L. Fu, C. L. Kane, and E. J. Mele, Phys. Rev. Lett. **98**, 106803 (2007).
- [2] J. E. Moore, and L. Balents, Phys. Rev. B **75**, 121306 (2007).
- [3] Y. L. Chen, J. G. Analytis, J. H. Chu, Z. K. Liu, S. K. Mo, X. L. Qi, H. J. Zhang, D. H. Lu, X. Dai, Z. Fang, S. C. Zhang, I. R. Fisher, Z. Hussain, and Z. X. Shen, Science **325**, 178 (2009).
- [4] D. Hsieh, Y. Xia, L. Wray, D. Qian, A. Pal, J. H. Dil, J. Osterwalder, F. Meier, G. Bihlmayer, C. L. Kane, Y. S. Hor, R. J. Cava, and M. Z. Hasan, Science **323**, 919 (2009).
- [5] T. Hirahara, Y. Sakamoto, Y. Takeichi, H. Miyazaki, S. I. Kimura, I. Matsuda, A. Kakizaki, and S. Hasegawa, Phys. Rev. B **82**, 155309 (2010).
- [6] J. G. A. Z. Alpichshev, J. H. Chu, I. R. Fisher, Y. L. Chen, Z. X. Shen, A. Fang, and A. Kapitulnik, arXiv:0908.0371 (2009).
- [7] K. K. Gomes, W. Ko, M. W, Y. Chen, Z.-X. Shen, and H. C. Manoharan, arXiv:0909.0921 (2009).
- [8] T. Zhang, P. Cheng, X. Chen, J.-F. Jia, X. Ma, K. He, L. Wang, H. Zhang, X. Dai, Z. Fang, X. Xie, and Q. Xue, arXiv:0908.4136 (2009).
- [9] C. Jozwiak, Y. L. Chen, A. V. Fedorov, J. G. Analytis, C. R. Rotundu, A. K. Schmid, J. D. Denlinger, Y. D. Chuang, D. H. Lee, I. R. Fisher, R. J. Birgeneau, Z. X. Shen, Z. Hussain, and A. Lanzara, Phys. Rev. B **84**, 165113 (2011).
- [10] D. Hsieh, Y. Xia, D. Qian, L. Wray, J. H. Dil, F. Meier, J. Osterwalder, L. Patthey, J. G. Checkelsky, N. P. Ong, A. V. Fedorov, H. Lin, A. Bansil, D. Grauer, Y. S. Hor, R. J. Cava, and M. Z. Hasan, Nature **460**, 1101 (2009).
- [11] A. Nishide, A. A. Taskin, Y. Takeichi, T. Okuda, A. Kakizaki, T. Hirahara, K. Nakatsuji, F. Komori, Y. Ando, and I. Matsuda, Phys. Rev. B **81**, 041309 (2010).
- [12] S. Souma, K. Kosaka, T. Sato, M. Komatsu, A. Takayama, T. Takahashi, M. Kriener, K. Segawa, and Y. Ando, Phys. Rev. Lett. **106**, 216803 (2011).
- [13] S. Y. Xu, L. A. Wray, Y. Xia, F. von Rohr, Y. S. Hor, J. H. Dil, F. Meier, B. Slomski, J. Osterwalder, M. Neupane, H. Lin, A. Bansil, A. Fedorov, R. J. Cava, and M. Z. Hasan, arXiv:1101.3985. (2011).
- [14] J. G. Analytis, J. H. Chu, Y. Chen, F. Corredor, R. D. McDonald, Z. X. Shen, and I. R. Fisher, Phys. Rev. B **81**, 205407 (2010).
- [15] Y. S. Hor, A. Richardella, P. Roushan, Y. Xia, J. G. Checkelsky, A. Yazdani, M. Z. Hasan, N. P. Ong, and R. J. Cava, Phys. Rev. B **79**, 195208 (2009).
- [16] J. G. Checkelsky, Y. S. Hor, R. J. Cava, and N. P. Ong, Phys. Rev. Lett. **106**, 196801 (2011).
- [17] J. G. Checkelsky, Y. S. Hor, M.-H. Liu, D.-X. Qu, R. J. Cava, and N. P. Ong, Phys. Rev. Lett. **103** 246601 (2009).
- [18] N. P. Butch, K. Kirshenbaum, P. Syers, A. B. Sushkov, G. S. Jenkins, H. D. Drew, and J. Paglione, Phys. Rev. B **81**, 241301 (2010).
- [19] D. X. Qu, Y. S. Hor, J. Xiong, R. J. Cava, and N. P. Ong, Science **329** pp. 821 (2010).
- [20] H. Peng, K. Lai, D. Kong, S. Meister, Y. Chen, X.-L. Qi, S.-C. Zhang, Z.-X. Shen, and Y. Cui, Nat. Mater. **9**, 225 (2010).
- [21] J. Chen, H. J. Qin, F. Yang, J. Liu, T. Guan, F. M. Qu, G. H. Zhang, J. R. Shi, X. C. Xie, C. L. Yang, K. H. Wu, Y. Q. Li, and L. Lu, Phys. Rev. Lett. **105**, 176602 (2010).
- [22] Y. S. Kim, M. Brahlek, N. Bansal, E. Edrey, G. A. Kapilevich, K. Iida, M. Tanimura, Y. Horibe, S. W. Cheong, and S. Oh, Phys. Rev. B **84**, 073109 (2011).
- [23] M. Liu, J. Zhang, C. Z. Chang, Z. Zhang, X. Feng, K. Li, K. He, L. L. Wang, X. Chen, X. Dai, Z.

- Fang, Q. K. Xue, X. Ma, and Y. Wang, Phys. Rev. Lett. **108**, 036805 (2012).
- [24] M. Liu, C. Z. Chang, Z. Zhang, Y. Zhang, W. Ruan, K. He, L. L. Wang, X. Chen, J. F. Jia, S. C. Zhang, Q. K. Xue, X. Ma, and Y. Wang, Phys. Rev. B **83**, 165440 (2011).
- [25] H. T. He, G. Wang, T. Zhang, I. K. Sou, G. K. L. Wong, J. N. Wang, H. Z. Lu, S. Q. Shen, and F. C. Zhang, Phys. Rev. Lett. **106**, 166805 (2011).
- [26] Z. Ren, A. A. Taskin, S. Sasaki, K. Segawa, and Y. Ando, Phys. Rev. B **82**, 241306 (2010).
- [27] S. Jia, H. Ji, E. Climent-Pascual, M. K. Fuccillo, M. E. Charles, J. Xiong, N. P. Ong, and R. J. Cava, Phys. Rev. B **84**, 235206 (2011).
- [28] J. Xiong, A. C. Petersen, D. Qu, R. J. Cava, and N. P. Ong, arXiv:1101.1315 (2011).
- [29] T. Arakane, T. Sato, S. Souma, K. Kosaka, K. Nakayama, M. Komatsu, T. Takahashi, Z. Ren, K. Segawa, and Y. Ando, Nat. Comm. **3**, 636 (2012).
- [30] A. A. Taskin, Z. Ren, S. Sasaki, K. Segawa, and Y. Ando, Phys. Rev. Lett. **107**, 016801 (2011).
- [31] Z. Ren, A. A. Taskin, S. Sasaki, K. Segawa, and Y. Ando, Phys. Rev. B **84**, 075316 (2011).
- [32] S. Matsuo, T. Koyama, K. Shimamura, T. Arakawa, Y. Nishihara, D. Chiba, K. Kobayashi, T. Ono, C. Z. Chang, K. He, X. C. Ma, and Q. K. Xue, Phys. Rev. B **85**, 075440 (2012).
- [33] H. Z. Lu, and S. Q. Shen, Phys. Rev. B **84**, 125138 (2011).
- [34] E. McCann, K. Kechedzhi, V. I. Fal'ko, H. Suzuura, T. Ando, and B. L. Altshuler, Phys. Rev. Lett. **97**, 146805 (2006).
- [35] P. Santhanam, S. Wind, and D. E. Prober, Phys. Rev. Lett. **53**, 1179 (1984).
- [36] A. Trionfi, S. Lee, and D. Natelson, Phys. Rev. B **72**, 035407 (2005).
- [37] P. A. Lee, A. D. Stone, and H. Fukuyama, Phys. Rev. B **35**, 1039 (1987).

Figure captions:

Fig. 1. Temperature dependence of resistivity in zero field of (a) bulk single crystal with thickness of 100  $\mu\text{m}$  and (b) nanoflake device with thickness of 200 nm. The room temperature ARPES spectrum of BSTS single crystal and the morphology of the nanoflake device under Scanning Electron Microscopy (SEM) are shown in the insets of (a) and (b) respectively.

Fig. 2. Angle-dependent magnetoresistance/conductance of bulk BSTS single crystals and nano-device.  $\theta$  is the angle between the direction of the magnetic field and the current flow plane. (a) and (b) Magnetoresistance of bulk BSTS single crystal and BSTS nanoflake device at several  $\theta$ s under 2K respectively. (c) and (d) Magnetoconductance in unit of  $e^2/h$  vs the perpendicular component of the magnetic field curves of bulk BSTS single crystal and BSTS nanoflake device respectively.

Fig. 3. Temperature-dependent magnetoconductance of BSTS single crystal and nanoflake device with  $\theta = 90^\circ$ . (a) Magnetoconductance change of bulk sample plotted with magnetic field at different temperatures in dot line. The 2D fitting curves are plotted in solid lines. The fitting curves do not agree with the experimental data well due to the intermixing effects. (b) The 2D WAL fitting curves agree very well up to 2 Tesla with the magnetoconductance change observed in nanoflake device at all temperatures from 2 K to 45 K. (c) and (d) The fitted values of  $L_\phi$  at different temperatures for single crystal and nanoflake device respectively. The fitting values follow the power law of temperature  $T^{-0.37}$  and  $T^{-0.51}$  respectively. (e) and (f) The fitted values of the prefactor  $\alpha$  at different temperatures for single crystal and nanoflake device respectively.

Fig 4 (a). Magnetofingerprint (UCF) signal  $\delta R$  vs magnetic field for the nanoflake device. At 2 K, we scan the field for three times with alternative field sweeping direction (the arrows). Seven UCF curves measured at temperatures between 2K to 10K were shown in the figures. (b) Temperature dependence of root mean square of the fluctuation of conductance. The solid line is the fitting curve using power law and the fitted power is -0.43.

Figure 1

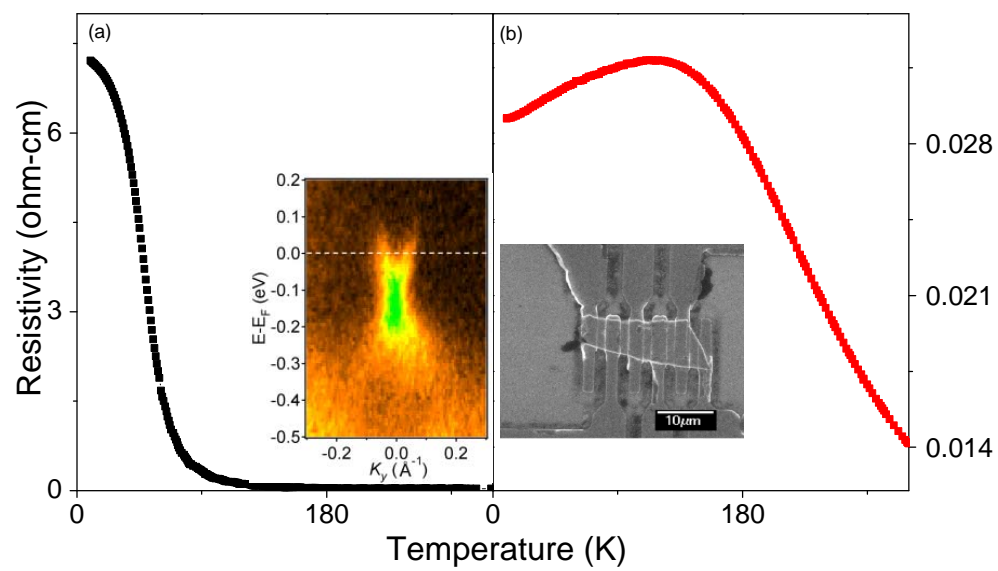


Figure 2

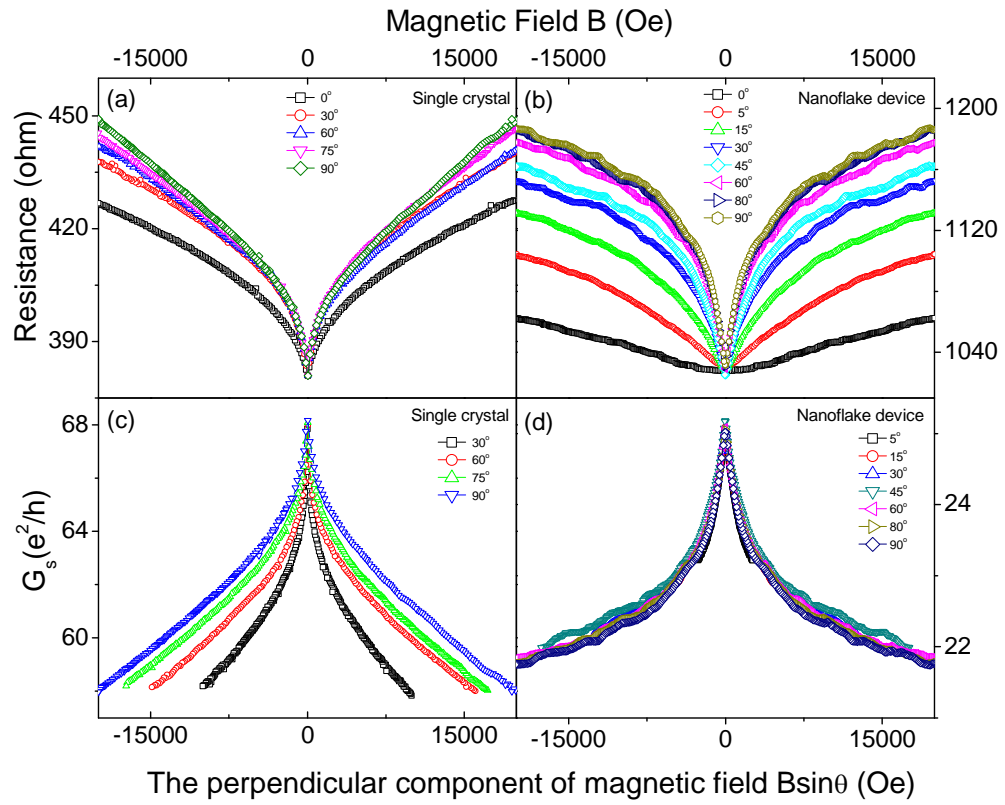




Figure 3

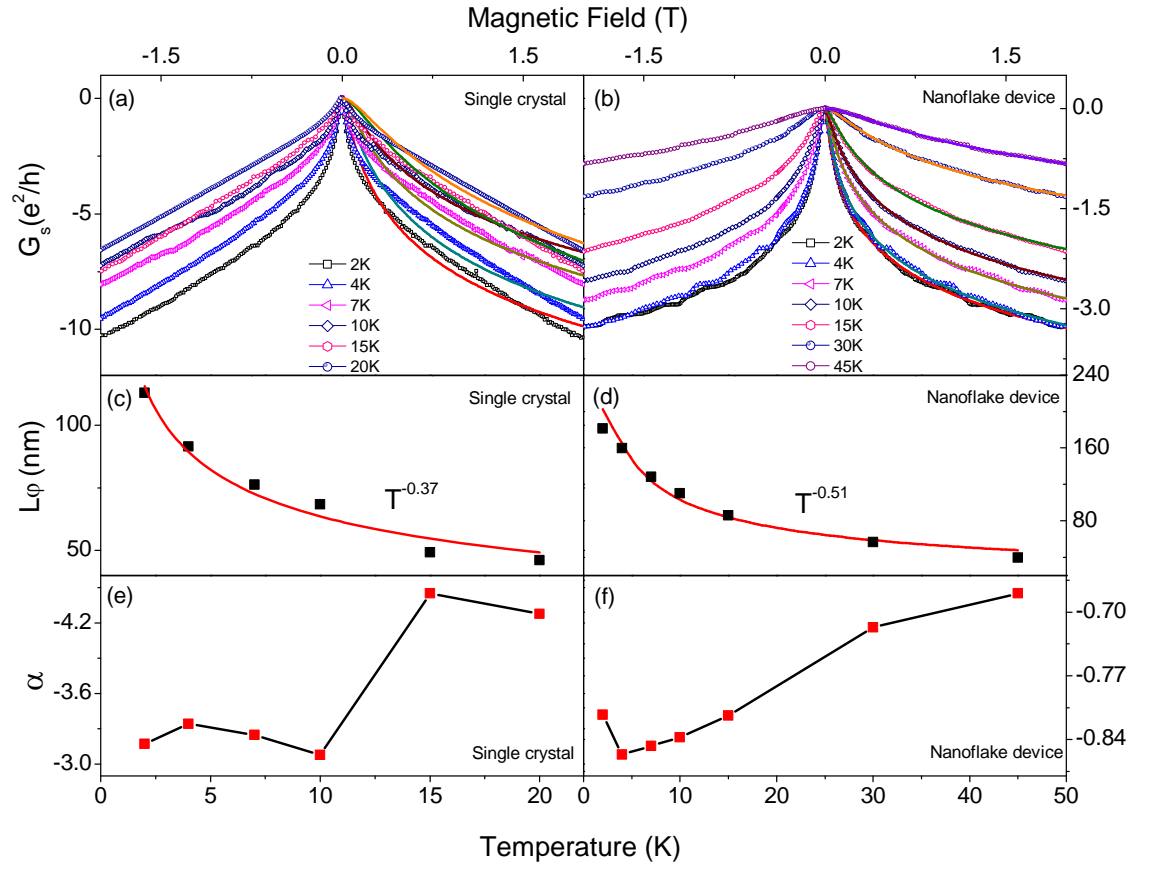


Figure 4

